ACS SENSORS

pubs.acs.org/acssensors

Article

An Approach for the Real-Time Quantification of Cytosolic Protein–Protein Interactions in Living Cells

Ilaria Incaviglia, Andreas Frutiger, Yves Blickenstorfer, Fridolin Treindl, Giulia Ammirati, Ines Lüchtefeld, Birgit Dreier, Andreas Plückthun, Janos Vörös, and Andreas M Reichmuth*

Cite This: *ACS Sens.* 2021, 6, 1572–1582

Read Online

ACCESS | Metrics & More | Article Recommendations

ABSTRACT: In recent years, cell-based assays have been frequently used in molecular interaction analysis. Cell-based assays complement traditional biochemical and biophysical methods, as they allow for molecular interaction analysis, mode of action studies, and even drug screening processes to be performed under physiologically relevant conditions. In most cellular assays, biomolecules are usually labeled to achieve specificity. In order to overcome some of the drawbacks associated with label-based assays, we have recently introduced "cell-based molography" as a biosensor for the analysis of specific molecular interactions involving native membrane receptors in living cells. Here, we expand this assay to cytosolic protein–protein interactions. First, we created a biomimetic membrane receptor by tethering one cytosolic interaction partner to the plasma membrane. The artificial construct is then coherently arranged into a two-dimensional pattern within the cytosol of living cells. Thanks to the molographic sensor, the specific interactions between the coherently arranged protein and its endogenous interaction partners become visible in real time without the use of a fluorescent label. This method turns out to be an important extension of cell-based molography because it expands the range of interactions that can be analyzed by molography to those in the cytosol of living cells.

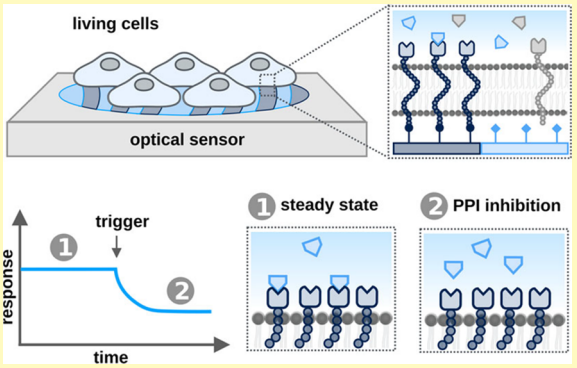

KEYWORDS: *cell-based assays, cell-based molography, protein-protein interactions, live-cell biosensors*

Molecular interactions between cellular proteins are commonly referred to as protein–protein interactions (PPIs) and are of central importance to every biological system.[1−3] PPIs play an active role in virtually all cellular functions including proliferation, apoptosis, cell metabolism, angiogenesis, metastasis, and immune destruction. Even though the significance of PPIs is widely recognized, high-affinity drugs that selectively modulate or disrupt the interaction between cytosolic proteins are still relatively rare compared to other drug classes.[4] This can be attributed to two main reasons. First, the contact surfaces involved in intracellular PPIs are typically devoid of deep grooves, clefts, or pockets that act as binding sites for natural ligands and could be easily exploited for the development of high-affinity small molecule drugs.[5] This makes the discovery of novel compounds inherently challenging. Second, there is a lack of suitable technologies for PPI analysis that work inside living cells. This is due to the fact that many cytosolic PPIs lack enzymatic functions related to their interaction, which is prohibitive for the development of broadly applicable assays.[6] Consequently, this latter point is worth expanding on.

Since the past years, biophysical and biochemical techniques including co-immunoprecipitation, single-molecule pull down, various fluorescence-based methods, NMR spectroscopy, X-ray crystallography, and surface plasmon resonance have been successfully used for the identification and analysis of fundamental interactions as well as for drug screening.[7−14] These techniques are essential to establish specificity for the protein of interest; however, most of them fail at providing a physiologically relevant context, which is crucial for the understanding of cellular processes and mode of action of drugs. In this respect, live-cell assays provide information needed to elucidate the effects of drug candidates in a physiological environment. However, they introduce the problem that the observed effect can no longer be exclusively attributed to the protein of interest.

To minimize this problem, several live-cell assays rely on genetically encoded fluorescent labels to track the movement of single proteins, enable kinetic analysis of PPIs, and for high-

Received: November 26, 2020
Accepted: March 11, 2021
Published: March 24, 2021

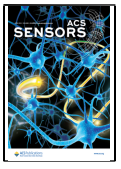

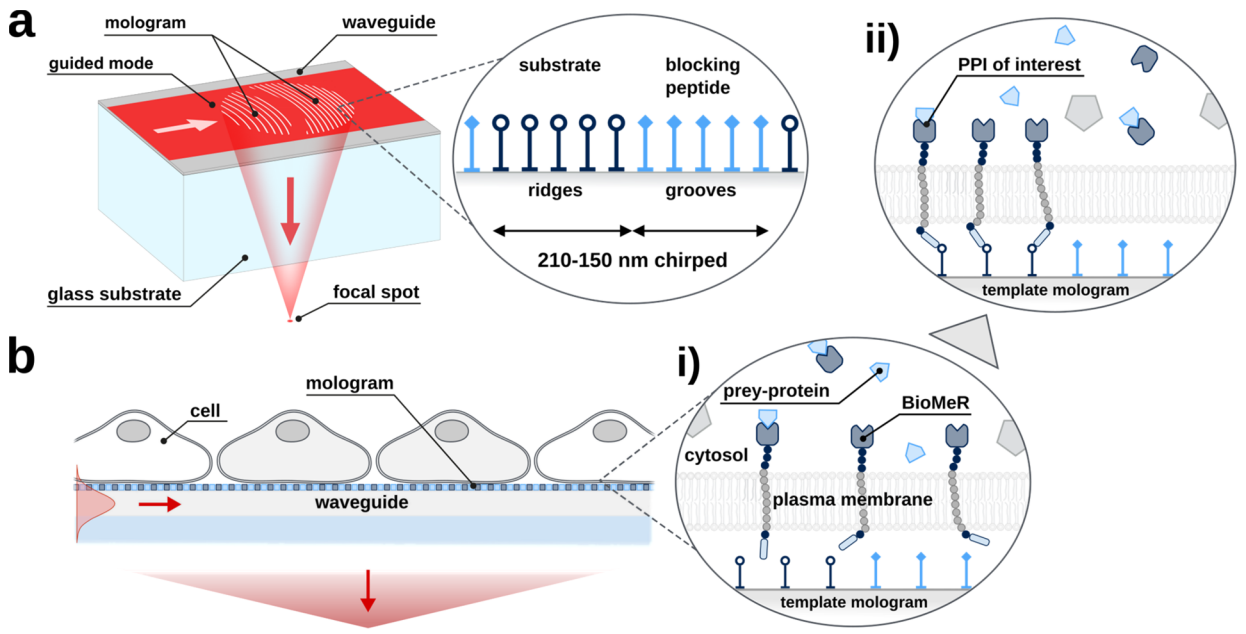

Figure 1. Principle of focal molography and application of biomimetic membrane receptors (BioMeRs) in cell-based molography. (a) Spatially defined 2D nanopattern of molecular binding sites, termed mologram, is generated on a single-mode optical waveguide using reactive immersion lithography (RIL). The ridges of the molographic pattern are functionalized with a substrate that allows for the binding of target molecules, whereas the grooves are backfilled with a blocking peptide. Binding of molecules to the mologram results in the physical manifestation of a diffraction grating in the shape of the mologram. When a laser beam is coupled onto the optical waveguide, the molographic grating scatters light at specifically bound molecules so that it constructively interferes in a diffraction-limited focal spot outside of the waveguide. The light intensity in the focal spot is measured to quantify molecular binding in real time. (b) Cells expressing the bait−protein of the PPI to be studied with a BioMeR are plated onto the sensor chip, which is functionalized with a molographic pattern. (i) Initially, no molographic signal is detectable as BioMeRs and endogenous proteins freely diffuse within the plasma membrane and the cytosol of cells. (ii) Binding of the BioMeRs to the template mologram on the chip via an extracellular tag transfers the molographic pattern to the inside of the cell. Molecular interactions of endogenously expressed cytosolic prey-proteins with BioMeRs can now be quantified in the focal spot of the mologram.

throughput screening of modulating compounds.[15−17] Nonetheless, label-based cellular assays have some drawbacks. For instance, resonant energy transfer (RET) biosensors necessitate for the fluorescent reporters to be in close proximity (<10 nm apart), which may require biomolecular optimization and makes it difficult to quantify PPIs.[18,19] Furthermore, they require that one or even both of the reaction partners are modified and recombinantly expressed, which could significantly perturb their function and interaction dynamics.

Recently, label-free live-cell biosensors have emerged as an attractive alternative to overcome some of these drawbacks.[20−22] In the case of optical systems, small refractive index changes in the adlayer above the sensor chip are measured by means of refractometry. Redistribution of cellular content within the first few hundred nanometers above the sensor surface results in an overall change of the bulk refractive index. Specific and nonspecific molecular interactions as well as morphological changes in the cell all cause refractive index changes. This feature has been successfully used to investigate complex signaling pathways,[23−27] differentiate the spreading kinetics of different cell types,[28] and even determine the dissociation constant of protein−ligand interactions.[29,30]

Here, we introduce a generalizable, quantitative live-cell assay for the analysis of cytosolic PPIs, which is based on the working principle of focal molography.[31−33] Focal molography is an optical system for molecular interaction analysis that is insensitive to nonspecific molecular interactions.[34] This unique property is achieved by the arrangement of binding sites into a regular (*i.e.*, coherent) pattern, termed the "mologram" (Figure 1a). The molographic pattern alternates ridges, which are usually made to contain high-affinity probes, and nonfunctional grooves, which act as an intrinsic reference.[35,36] Binding of target analytes to the probes on the ridges results in the physical manifestation of a diffraction grating in the shape of the mologram. The mologram is designed such that the light of a guided laser beam is scattered at specifically bound molecules and constructively interferes in a diffraction-limited focal spot.[31,33] The light intensity in the focal spot is measured to quantify molecular binding in real time.[37] Meanwhile, the light scattered by randomly bound molecules does not contribute to this effect.

Based on this principle, we previously introduced cell-based molography, where specific molecular interactions between membrane proteins and cytosolic proteins are measured in living cells.[38] In cell-based molography, the molographic pattern is established within the membrane of living cells (Figure 1b). This is achieved by creating a molographic pattern made of a ligand of the membrane protein of interest on the surface of a sensor chip. When living cells are plated onto the sensor chip, the targeted membrane protein aligns to the molographic pattern while still residing in the plasma membrane. Specific molecular interactions between the membrane protein and cytosolic proteins can be measured via the intensity of the molographic focal spot. In contrast, nonspecific molecular interactions as well as changes to bulk properties of the cells (*e.g.*, mass or volume) and their environment are suppressed. As a result, cell-based molography enables the quantitative analysis of membrane proteins with their endogenous interaction partners in real time. This is fundamentally different from refractometric biosensors intro-

https://doi.org/10.1021/acssensors.0c02480
ACS Sens. 2021, 6, 1572−1582

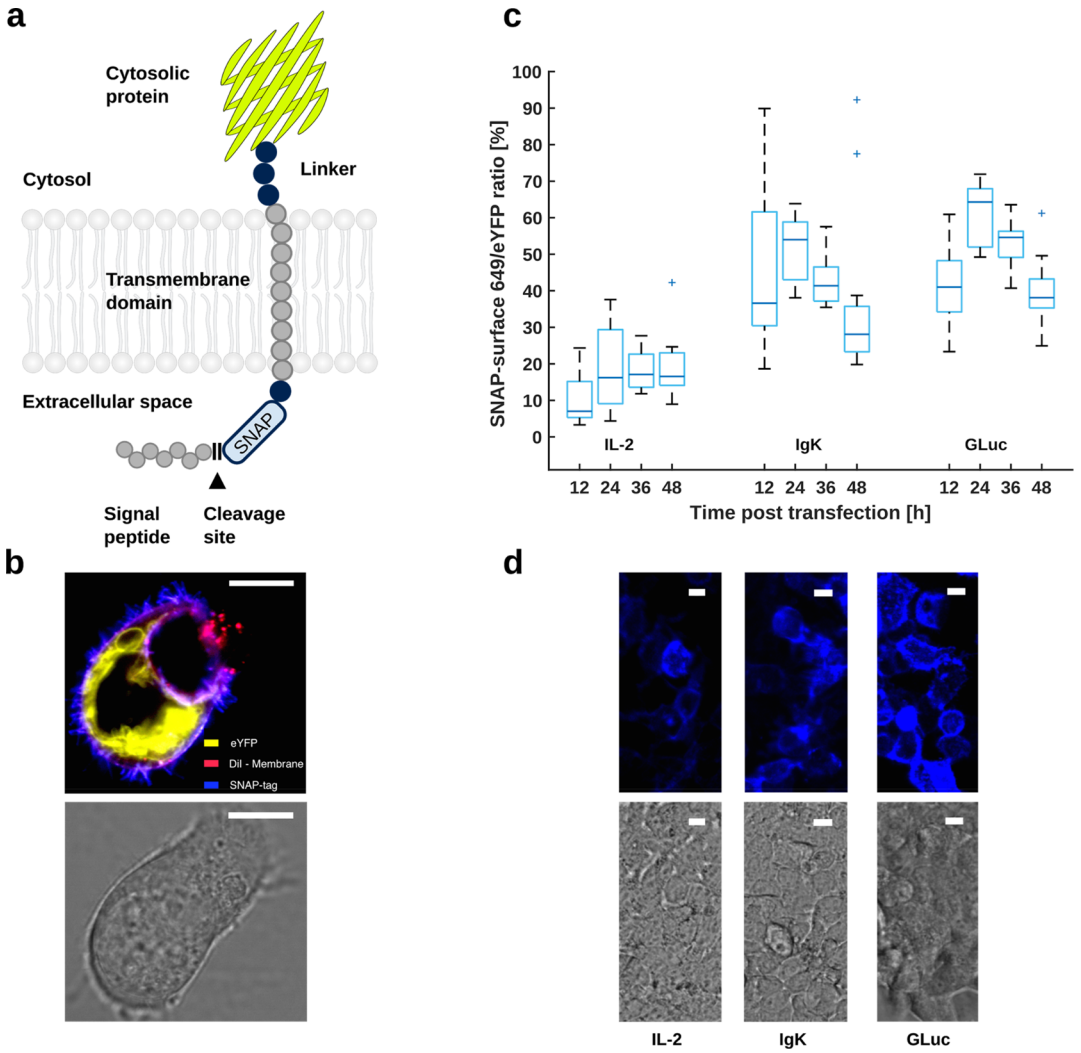

Figure 2. Integration of BioMeRs across the cell membrane using different signal peptide sequences. (a) BioMeRs consist of an N-terminal cleavable signal peptide that initiates BioMeR translocation across the cell membrane, followed by an extracellular autoreactive SNAP-tag that can bind to a template mologram. A single spanning transmembrane domain connects the SNAP-tag to an intracellular domain that acts as a probe for cytosolic molecules and proteins. The intracellular domain defines the specificity of the BioMeR and can be tailored accordingly: *e.g.*, with a protein or protein domain to monitor specific molecular interactions, with an intracellular antibody (intrabody) or other specificity modules that can be expressed intracellularly, *e.g.*, with DARPins[47] to report the temporal occurrence of specific cytosolic proteins or with an enzyme to report enzymatic activity over time. (b) Merged confocal laser scanning microscope (CLSM) (488, 561, and 640 nm) and bright-field images of membrane-stained HEK293 cells expressing eYFP-BioMeRs. The membrane-impermeable SNAP-reactive surface 649 dye reveals the correct orientation across the cell membrane. The SNAP-tag protein is found on the extracellular side of the plasma membrane and eYFP on the intracellular side. Some BioMeRs are falsely targeted to subcellular locations other than the plasma membrane. Scale bar: 10 μm. (c) Staining of the extracellular SNAP-tag with the cell-impermeable dye SNAP-surface 649 reveals membrane-targeting efficiency of IL-2, IgK, and GLuc signal peptide sequences, reported as a SNAP/eYFP fluorescence ratio. Data represent mean ± s.d. of n = 12 repeats collected over three individual experiments. Outliers are marked with a plus "+" and were due to an increased number of dead cells. (d) CLSM and bright-field images (640 nm) of SNAP-surface 649-stained HEK293 cells expressing eYFP-BioMeRs with different export sequences 24 h after transfection. Scale bars: 10 μm.

duced earlier, which display an overall response encompassing a variety of cellular events. As such, the signal acquired by refractometric biosensors is usually expressed as a relative response with respect to a baseline signal rather than directly quantifying the interaction under study.[23,24,39,40] On the other hand, cell-based molography exclusively detects the interaction of a protein of interest with its specific endogenous interaction partners but does not report the sometimes dramatic cytoskeleton reorganization in response to the specific interaction. For this reason, cell-based molography is capable of providing a quantitative signal that directly correlates to the mass binding to the sensor surface and can therefore be expressed in pg/mm^2 units.[38]

In this work, we expand the idea of cell-based molography to interactions between cytosolic proteins and provide a tool for the quantification of virtually any cytosolic PPI in living cells in real time. This is achieved by synthetically tethering the cytosolic protein of choice (*i.e.*, the bait) to a membrane-spanning linker. The cytosolic portion of this artificial membrane protein serves as a receptor for its endogenous interaction partners (*i.e.*, the prey), while the extracellular portion allows for binding to the template mologram (Figure 1b). We name this construct a biomimetic membrane receptor or, in short, BioMeR. A similar design has previously been employed to detect protein−protein interactions in living cells using a fluorescent approach.[41]

https://doi.org/10.1021/acssensors.0c02480
ACS Sens. 2021, 6, 1572−1582

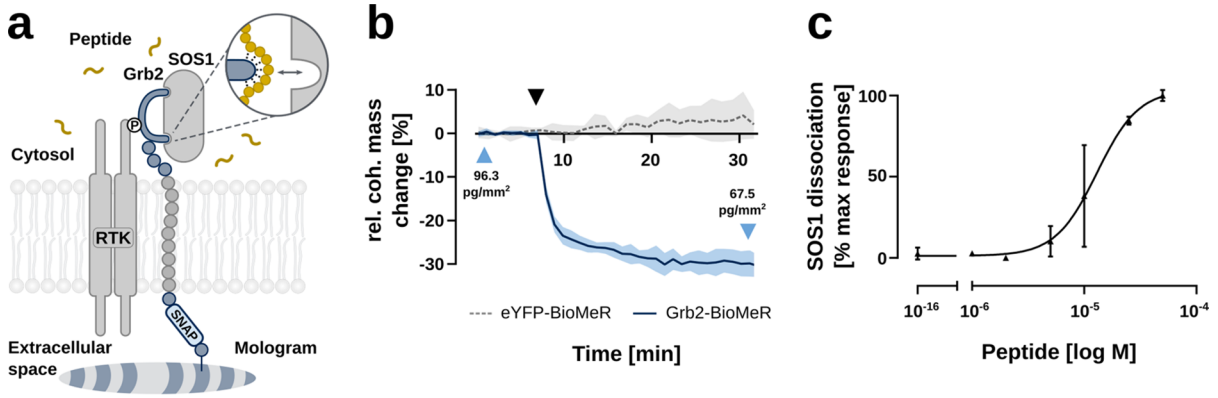

Figure 3. Grb2-BioMeRs report peptide induced cytosolic PPI disruption in HEK293 cells. (a) Grb2-BioMeRs are covalently bound to a template mologram using an extracellular SNAP-tag. The constitutively bound guanine nucleotide exchange factor SOS1 is then disrupted by a cell-penetrating peptide that binds to the N-terminal SH3 domain of Grb2. Unbinding of SOS1 from the coherently arranged Grb2-BioMeRs can then be observed molographically. (b) Stimulation of HEK293 cells expressing Grb2-BioMeRs with 50 μM (black arrow) of the Grb2-SOS1 disruptive peptide leads to a rapid decrease of the molographic signal. In contrast, the molographic signal of cells expressing eYFP-BioMeRs remains unaffected. The figure shows the mean equivalent coherent mass density modulation of four individual mologrames of one representative experiment. (c) Cells expressing Grb2-BioMeRs were treated with increasing concentrations of the disruptive peptide. The half maximal effective peptide concentration after 30 min was found to be approximately 13 $\pm$ 2.5 μM. The area under the curve (AUC) was plotted as a function of peptide concentrations. Data represent mean $\pm$ s.d. of $n \geq 2$ individual experiments.

In this paper, we present the experimental realization of molography-based cytosolic PPI analysis in living cells using BioMeRs. We rationally designed BioMeRs and optimized their membrane integration by mimicking the structural features of naturally occurring membrane receptors. Then, we exemplified their broad applicability with two model systems: first, by detecting the disruption of an intracellular protein complex through an unlabeled peptide that autonomously diffuses into cells; and second, by quantifying the post-translational modification of endogenous ERK1/2 resulting from upstream MEK inhibition by small molecules.

RESULTS

Efficient Integration of BioMeRs across the Cell Membrane Depends on the Signal Peptide Sequence. In order to measure cytosolic PPIs by molography, we designed BioMeRs such that one interaction partner of the PPI of interest acts as an intracellular probe that is coherently aligned through the cell membrane by the template mologram. The design mimics structural features of natural transmembrane proteins as follows (Figure 2a): an N-terminal signal peptide sequence ensures translocation of the newly synthesized BioMeR across the membrane. The signal peptide is followed by a molecular tag, for example, an autoreactive SNAP-tag, which is also translocated to the extracellular side and enables straightforward covalent binding to a SNAP-reactive substrate on the template mologram. A single spanning PDGFR-β transmembrane domain is responsible for retaining the protein within the plasma membrane. A flexible linker on the cytosolic side connects the N-terminus of a cytosolic protein to the transmembrane helix and facilitates precessional freedom.[42] Once the protein has been inserted into the membrane, the signal peptide is cleaved off by signal peptidase and is therefore absent in the mature protein.[43] This design ensures the correct orientation of the BioMeR across the plasma membrane, facilitates the alignment to the template mologram, and allows to loosely retain the cytosolic protein in the proximity of the membrane. This design can then be genetically encoded in a plasmid (for details, refer to Table 1 in the Methods section) that enables the expression of the respective BioMeR by the cell after transfection (Figure 2b). Since only the correctly oriented BioMeRs, which are residing in the plasma membrane, participate in the molographic assay, their efficient integration into the plasma membrane is crucial for the working principle of the method.

Therefore, from the various signal peptide sequences identified today, we tested different sequences that were previously reported to be highly effective at initiating protein secretion.[44−46] These signal sequences included a modified interleukin-2 (IL-2) signal peptide, a mouse immunoglobulin κ light chain (IgK) peptide, and a *Gaussia* Luciferase (Gluc) signal peptide. We employed a construct in which a yellow fluorescent protein (YFP) was fused to the C-terminus of the transmembrane helix (termed eYFP-BioMeR), which was transiently expressed in HEK293 cells, and we screened signal peptides for membrane integration efficiency (Figure 2c). Thereby, the ratio of intracellular YFP to extracellular SNAP-tag fluorescence (where the SNAP-tag was coupled to SNAP-reactive surface 649 dye) served as a measure for membrane integration efficiency, which is independent from the overall amount of the expressed protein. Out of the three tested signal peptides, we found Gluc to be the most efficient at correctly integrating BioMeRs into the plasma membrane (Figure 2c), with around 60% of BioMeRs being correctly integrated into the membrane, as well as for the overall protein expression (Figure 2d). Therefore, Gluc was used as the preferred export sequence for constructing all subsequent BioMeRs.

Cytosolic Proteins Can Serve as Artificial Receptors for Their Native Interaction Partner. While addressing the lack of small molecule-binding sites in many cytosolic targets, a significant advancement was the understanding that the affinity of PPIs is largely driven by specific residues, called hot regions, as opposed to the entire contact surface of the proteins. Accordingly, most PPIs are mediated by either a linear peptide stretch of one protein interacting with such a hot region on the partner protein (domain−peptide interaction) or a single hot patch on the surface of both interacting proteins (domain−domain interaction).[48,49] Because of the prominent role of hot

https://doi.org/10.1021/acssensors.0c02480
ACS Sens. 2021, 6, 1572−1582

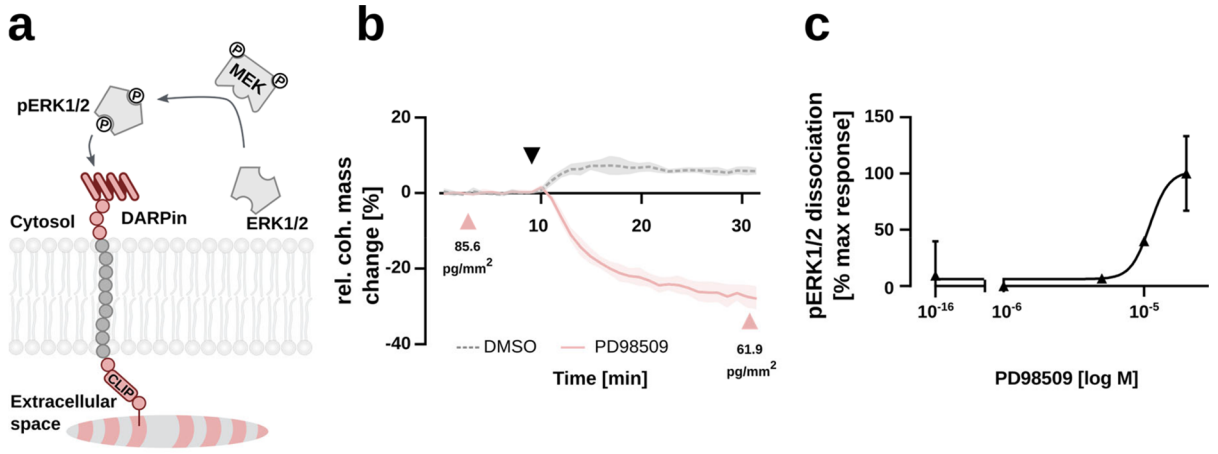

Figure 4. Label-free monitoring of ERK1/2 phosphorylation in HEK293 cells. (a) pE59-BioMeRs are covalently arranged to a template mologram using an extracellular CLIP-tag. Due to the high affinity and high unbinding rate for pERK1/2 but not unphosphorylated ERK1/2, the intracellular pE59 DARPin can accurately track ERK1/2 phosphorylation. (b) Inhibition of the upstream kinase MEK with 20 μM of PD98509 (first arrow) decreases the intracellular concentration of pERK1/2, which is detected as a decrease in the mologram signal. The figure shows the mean equivalent coherent mass density modulation of four individual mologrames of a representative experiment. (c) Cells expressing pE59-BioMeRs were treated with increasing concentrations of PD98509. The half maximal effective peptide concentration was estimated to be about 8.2 ± 5.4 μM. The area under the curve (AUC) was plotted as a function of MEK inhibitor concentration. Data represent mean ± s.d. of $n \geq 1$ individual experiments.

segments in PPIs, low molecular weight peptidomimetics have recently been used as drugs for modulating specific interactions.[50] Peptidomimetics are characterized by sufficient conformational flexibility and metabolic stability for translocation across the cell membrane while providing sufficient affinity to bind to flat PPI interfaces.[51]

To demonstrate that BioMeRs are suited to study PPI inhibitors in living cells, we constructed a growth factor receptor-bound protein 2 (Grb2)-BioMeR (Figure 3a) and expressed it in HEK293 cells. Grb2 is a ubiquitously expressed adaptor protein that takes part in the upstream MAP kinase pathway. For this reason, Grb2 is essential to a variety of basic cellular functions, such as cell cycle progression and cell motility.[52] Among others, it links membrane-bound receptor tyrosine kinases (RTKs) to the activation of Ras and its downstream kinases via the guanine nucleotide exchange factor Son of Sevenless 1 (SOS1).[53,54] The constitutively bound Grb2-SOS1 complex is naturally found close to the cell membrane; therefore, it was chosen as an ideal proof of principle for molographic PPI disruption monitoring.

To this end, we stimulated HEK293 cells stably expressing Grb2-BioMeRs or eYFP-BioMeRs (Figure 3b) with 50 μM of a previously reported cell-penetrating peptide that blocks the N-terminal SH3 domain of Grb2.[55] Upon stimulation of Grb2-BioMeRs, we observed a rapid decrease in the molographic signal over the course of 25 min (Figure 3b). In comparison, stimulation of eYFP-BioMeRs with the same peptide led to no change in the molographic signal, demonstrating that the peptide evoked a specific response at the Grb2-BioMeR. In cell-based mology, any membrane-bound and cytosolic molecule that is not coherently arranged to the template mologram (*i.e.,* that does not interact with the BioMeR) yields no measurable molographic signal.[38] Therefore, it remains unclear whether the peptide evoked an additional off-target effect on other proteins. Nevertheless, the observed ∼30% signal decrease (28.8 pg/mm^2) corresponds to a protein that is constitutively bound to Grb2 and displaced by the peptide. Assuming that all Grb2-BioMeRs were occupied by SOS1 that were displaced by the peptide, we can estimate the number and molecular weight of all the coherently arranged proteins. With a molecular weight of 152 kDa, SOS1 would thus account for 74,000 coherently arranged proteins per cell or ∼30% of a 500 kDa protein complex where Grb2-BioMeR accounts for approximately 52 kDa. The remaining ∼300 kDa may be explained by the presence of RTKs (their molecular weights range from approximately 130−190 kDa, and they usually occur as dimers when activated[56]) that are combined with the Grb2-BioMeR.

Even though cell-based mology can quantify the amount of coherently arranged proteins in a cell, it is more difficult to determine the absolute number of a specific protein in a protein complex. This is because first, there is no necessity for the theoretical stoichiometric relationship of proteins to hold in reality. This effect becomes somewhat less of a concern when BioMeR expression is closer to endogenous protein expression levels. Second, there may be other proteins coherently arranged to the Grb2-BioMeR than the ones suggested. Therefore, for future cell-based molographic systems, we suggest the binding of a molecule with well-known molecular weight or induced unbinding of a portion of a biological complex as a universal method to calibrate the molographic signal in terms of molecular masses of the involved species. Though unbinding of SOS1 was detectable molographically, binding of the low molecular weight peptide (∼3 kDa) remained invisible in the molographic signal, which is likely to be due to the insufficient mass resolution of the current setup. The half maximal effective peptide concentration (EC50) of 13 μM (Figure 3c) compared reasonably well to the previously reported value of ∼15 μM for half maximal proliferation inhibition in the cell culture.[55]

Compared to RET-based assays, BioMeR-assisted cell-based mology does not impose constraints on the design of the assay itself (*e.g.,* distance of fluorescent reporters) and requires no modifications on the prey−protein, which is potentially advantageous for assay development. On the other hand,

https://doi.org/10.1021/acssensors.0c02480
ACS Sens. 2021, 6, 1572−1582

BioMeRs closely confine the bait−protein to the plasma membrane, which could alter the activity of certain proteins.

Intracellular Direct Binding Assay Quantifies Post-Translational Modification of Native Proteins in Real Time. Post-translational modifications (PTMs) are fundamental regulators of the cell cycle and signal transduction with high pathological relevance.[57,58] Traditionally, PTMs have been studied in fixed cells or lysates with limited temporal resolution. PTMs can neither be directly studied using gene expression analytics nor fluorescent tags, making it notoriously difficult to study PTMs in living cells.[59] For these reasons, binding molecules that are functional in the cytosol and specifically recognize target proteins have gained increasing attention in the past years.[47,60] Besides therapeutic applications, they have also been employed as fluorescent biosensors to image PTMs. However, high background fluorescence or the necessity to also modify the protein under study are major limiting factors of fluorescence-based methods.[59] Cell-based molography is intrinsically insensitive to off-target molecular interactions of the soluble protein, allowing for direct binding assays in living cells. Conversely, off-target interactions of the BioMeR can be tested in control experiments.

Therefore, we designed a specific BioMeR that serves as a cytoplasmically active binding protein to quantify the post-translational phosphorylation of endogenous ERK1/2 in real time (Figure 4a). This BioMeR is based on the pE59 DARPin,[61] which specifically distinguishes pERK from ERK[61] and was used as a real-time in vivo sensor before.[62] We expressed the pE59-BioMeR in HEK293 cells and diminished ERK1/2 phosphorylation by inhibiting the upstream kinase MEK with the inhibitor PD98509. Initially, phosphorylated ERK1/2 (pERK1/2) is found in an equilibrium state of bound and unbound pERK1/2 with respect to the pE59-BioMeR (Figure 4b). Upon inhibition of MEK with 20 μM of PD98509, the phosphorylation of ERK is diminished and the intracellular concentration of pERK1/2 is decreasing. The molographic signal from the pE59-BioMeR decreases rapidly upon inhibition of MEK (Figure 4b, first black arrow) and reaches a plateau after ∼30 min, which is in good agreement with the previously reported temporal succession of ERK phosphorylation.[63] In comparison, treatment with an equivalent amount of DMSO used to dissolve the MEK inhibitor does not lead to a significant drop in the molographic signal. Instead, we observed a slight signal increase after addition of DMSO (Figure 4b). This increase in signal reported through the pE59-BioMeR may be caused by the mechanical stimulation of the cells upon manual compound addition, which leads to the well-known activation of the MAP kinase pathway or by the decrease in overall refractive index upon dilution of previously DMSO-corrected measurement buffer in the measurement chamber.

To quantify the number of pERK1/2 prior to MEK inhibition, we assume complete dissociation of pERK1/2 from the pE59-BioMeR after 30 min. In this case, the signal drop of ∼28% or 23.7 pg/mm^2 corresponds to approximately 215,000 pERK1/2 proteins per cell, which were previously bound by the BioMeR. We estimated the half maximal inhibitory concentration (IC50) of PD98509 to be about 8.2 μM (Figure 4c), which is in good agreement with the value reported by the manufacturer (7 μM). It is important to note that pE59-BioMeR cells only responded in the first few passages after thawing the cells. Cells that were passaged multiple times gave no reproducible response. We hypothesize that this effect might be due to a change in expression patterns along the MAP kinase pathway induced by the pE59 DARPin.

SUMMARY AND OUTLOOK

In summary, we have established cytosolic PPI analysis using cell-based molography in living cells. For this purpose, we developed BioMeRs consisting of an extracellular SNAP- or CLIP-tag that can bind covalently to a template mologram, followed by a single span transmembrane domain that connects to a cytosolic bait−protein. When living cells are plated on a molographic sensor, the BioMeRs align to the template mologram and transfer its pattern to the cytosolic space. There, interactions with the bait−protein can be measured. We developed two model systems on the basis of the well-known MAP kinase pathway to demonstrate the working principle of BioMeR-assisted cell-based molography. In the first model system, we disrupted the interaction of Grb2-BioMeRs and SOS1 with a blocking peptide, and we quantified the induced dissociation of SOS1 with the molographic setup. In the second model system, we employed a specific DARPin-based BioMeR to monitor the unbinding of phosphorylated ERK1/2 from the DARPin upon upstream kinase inhibition. While these models exemplify that BioMeRs can be constructed by endogenous or exogenous proteins to investigate molecular interactions of target proteins, one needs to keep in mind that by the nature of cell-based molography, concurrent coherent processes cannot be distinguished. Additionally, off-target interactions, such as the disruption of other PPIs by a drug under investigation, are not reported.

Due to the label-free signal acquisition of cell-based molography, the protein of interest requires no molecular modifications and is expressed endogenously. Therefore, the design of specific BioMeRs targeting a protein of interest is not restricted by spectral overlaps or by the location of the molecular modification. On the other hand, BioMeR-assisted cell-based molography does not allow for interaction analysis with proteins from intracellular locations other than the cytosol and plasma membrane. Moreover, since BioMeRs are covalently linked to a template mologram, subcellular relocalization of proteins upon interaction is spatially restricted. The linker itself could also prove to be disadvantageous especially when close to a binding pocket. In addition, the cytosolic interaction of interest is artificially brought in proximity of the plasma membrane, which could be unsuitable for certain investigations. Finally, calibration of the molographic signal in terms of molecular masses of the involved species is still unsolved, which makes the evaluation of BioMeR occupation challenging. All in all, we foresee BioMeRs to be especially advantageous when derived from cytoplasmically active binding proteins, such as DARPins, to study PTMs and contribute to PTM-specific drug discovery processes. Finally, on the present proof of principle setup, the limit of detection in terms of mass was in the order of 10 pg/mm^2. However, we foresee detection limits in the 300 fg/mm^2 range, which has already been demonstrated for non-cell-based molography.[33] This would not only allow for the monitoring of PPIs at much lower expression levels but also enable molecular interaction analysis on the single-cell level by decreasing the diameter of the mologram from ∼400 to 10−20 μm.

MATERIALS AND METHODS

Cell culture medium Dulbecco's modified Eagle's medium (DMEM) high glucose (4.5 g/L) with L-glutamine (BioConcept, Switzerland),

https://doi.org/10.1021/acssensors.0c02480
ACS Sens. 2021, 6, 1572−1582

Table 1. Amino Acid Sequences of Individual BioMeR Subdomains

feature	sequence (N- to C-terminus)
IL-2 signal peptide	MRMQLLLLIALSLALVTNS
IgK signal peptide	METDTLLLWVLLLWVPGSTGD
Gluc signal peptide	MGVKVLFALICIAVAEA
SNAP-tag	MDKDCEMKRTTLDSPLGKLELSGCEQGLHRIIFLGKGTSAADAVEVPAPA AVLGGPEPLMQATAWLNAYFHQPEAIEEFPVPALHHPVFQQESFTRQVL WKLLKVVKFGEVISYSHLAALAGNPAATAAVKTALSGNPVPILIPCHRVV QGDLDVGGYEGGLAVKEWLLAHEGHRLGKPGLG
CLIP-tag	MDKDCEMKRTTLDSPLGKLELSGCEQGLHRIIFLGKGTSAADAVEVPAPA AVLGGPEPLIQATAWLNAYFHQPEAIEEFPVPALHHPVFQQESFTRQVLW KLLKVVKFGEVISESHLAALVGNPAATAAVNTALDGNPVPILIPCHRVVQ GDSDVGPYLGGLAVKEWLLAHEGHRLGKPGLG
PDGFR-β transmembrane domain	AVGQDTQEVIVVPHSLPFKVVVISAILALVVLTIISLIILIMLWQKKPR
linker	GGGGSGGGGSGSAGSAAGSGEFGGGGSGGGGSG
eYFP	MVSKGEELFTGVVPILVELDGDVNGHKFSVSGEGEGDATYGKLTLKFIC TTGKLPVPWPTLVTTFGYGLQCFARYPDHMKQHDFFKSAMPEGYVQER TIFFKDDGNYKTRAEVKFEGDTLVNRIELKGIDFKEDGNILGHKLEYNYN SHNVYIMADKQKNGIKVNFKIRHNIEDGSVQLADHYQQNTPIGDGPVLLP DNHYLSYQSALSKDPNEKRDHMVLLEFVTAAGITLGMDELYK
Grb2	MEAIAKYDFKATADDELSFKRGDILKVLNEECDQNWYKAELNGKDGFI PKNYIEMKPHPWFFGKIPRAKAEEMLSKQRHDGAFLIRESESAPGDFSLS VKFGNDVQHFKVLRDGAGKYFLWVVKFNSLNELVDYHRSTSVSRNQQI FLRDIEQVPQQPTYVQALFDFDPQEDGELGFRRGDFIHVMDNSDPNWW KGACHGQTGMFPRNYVTPVNRNV
pE59 DARPin	DLGKKLLEAARAGQDDEVRILMANGADVNALDEDGLTPLHLAAQLGHL EIVEVLLKYGADVNAEDNFGITPLHLAAIRGHLEIVEVLLKHGADVNAQ DKFGKTAFDISIDNGNEDLAEILQ

Lipofectamine 3000, opti-MEM I (1X), versene 1:5000 (1X), fetal bovine serum (FBS), G418, phosphate-buffered saline, pH 7.4 (PBS, catalog number: 10010-015), and Hank's balanced salt solution with calcium and magnesium (HBSS, catalog number: 14025-050) were purchased from Life Technologies Europe (Zug, Switzerland). TPP 6-well tissue culture plates and tissue culture flasks were from Faust Laborbedarf AG (Schaffhausen, Switzerland). The amine reactive SNAP-tag substrate O^6-benzylguanidine (BG-GLA-NHS) and SNAP surface 649 dye were purchased from Bioconcept AG (Allschwil, Switzerland). The amine reactive CLIP-tag substrate O^6-benzylcytosine (BC-GLA-NHS) was custom synthesized by KareBay Biochem (Monmouth Junction, NJ, USA). The GRGDSPGSC-(DBCO) peptide was custom synthesized by LifeTein, LLC (Somerset, NJ, USA), whereas the cell-penetrating peptide (KKWKMRRNPFWIKIQRC-CGIRVVDNSPPPPLPPRRRRSAPSPTRV-amide) was custom synthesized by GenicBio Ltd. (Shanghai, China). Azido-PEG4-NHS was obtained from Jena Bioscience (Jena, Germany). PD98509 was purchased from Tocris Bioscience (Bristol, U.K.). All other chemicals were purchased from Sigma–Aldrich Chemie GmbH (Buchs SG, Switzerland). The PAA-g-PEG-NH-PhSNPPOC copolymer, used as a biocompatible coating, was a kind gift of Roche (Basel, Switzerland). Zeptosens thin-film optical waveguides with a 145 nm Ta_2O_5 layer with the in- and out-coupling gratings covered with a 1 μm-thick layer of SiO_2 by IMT Masken und Teilungen AG (Greifensee, Switzerland) were a kind gift of Roche (Basel, Switzerland).

Cell Culture. HEK293 wild-type cells were cultured in a DMEM containing 10% v/v fetal bovine serum at 37 °C in a cell incubator with 5% CO_2. Cells stably expressing Grb2- and pE59-BioMeRs were cultured in a medium additionally supplemented with 600 μg/mL G418.

Stable Cell Line Generation. For the generation of transiently expressing eYFP-BioMeR cells, HEK293 cells were seeded in six-well plates at 600–800 k cells/well in 2 mL of culture media and transfected using the Lipofectamine 3000 transfection reagent according to the manufacturer's protocol. In order to establish stable Grb2- and pE59-BioMeR cell lines, transiently transfected cells were grown in medium supplemented with 1 mg/mL G418 for approximately 20 days. Afterward, neomycin-resistant cells were stained using a SNAP- or CLIP-surface 649 dye and selected by flow cytometry.

Plasmids. Plasmids encoding for different BioMeRs were purchased from Invitrogen GeneArt Gene synthesis service by Thermo Fisher Scientific. All synthetic genes were assembled from synthetic oligonucleotides and/or PCR products and inserted into a pcDNA3.1(+) vector backbone by the manufacturer. The plasmid DNA was purified from bacteria, the concentration was determined by UV spectroscopy, and the final constructs were verified by sequencing by the manufacturer. Plasmids were delivered in TE buffer (10 mM Tris–HCl, pH 8.0, 1 mM EDTA) at a concentration of 1 mg/mL and stored at 4 °C. The amino acid sequences of the individual BioMeR subdomains are displayed in Table 1.

Preparation of Sensor Chips. Thin-film optical waveguides were treated using a protocol reported previously.[32] Briefly, waveguides were washed with 0.1% aqueous Tween-20, followed by ultrasound-assisted washing in MilliQ water, isopropanol, and toluene. The chips were then immersed in warm Hellmanex III for 1 min and thoroughly rinsed with MilliQ water. Afterward, the chips were cleaned in ultrasound-assisted highly oxidizing Piranha solution (H_2SO_4/H_2O_2 7:3) for 30 min and thoroughly washed with MilliQ water. Chips were centrifuge-dried at 800 rcf for 2 min and activated by oxygen plasma. After plasma treatment, the chips were immediately immersed in the PAA-g-PEG-NH-PhSNPPOC graft copolymer coating solution (0.1 mg/mL in 1 mM HEPES pH 7.4) for 60 min for copolymer adlayer formation. To fully passivate the layer, the chips were washed with MilliQ water and ethanol and immersed in a 25 mM solution of methyl chloroformate in anhydrous acetonitrile containing 2 equiv of *N*,*N*-diisopropylethylamine for 5 min. The coated chips were washed with ethanol and MilliQ water and blow dried by a nitrogen jet. Prepared sensor chips were stored in the dark at 4 °C until further use.

Preparation of Template Mologrames. Mologrames were prepared following the standard reaction immersion lithography process described previously.[32,64] In short, a previously copolymer-

https://doi.org/10.1021/acssensors.0c02480
ACS Sens. 2021, 6, 1572–1582

coated sensor chip was placed in a custom holder. The phase mask used to generate the mologram was aligned using an alignment help, and the gap between the chip and phase mask was filled with a solution of 0.1% v/v hydroxylamine in DMSO. Then, a photolithographic exposure was conducted at 405 nm with a dose of 2000 mJ/cm^2 in a custom-built setup to create the molographic pattern. After illumination, the chip was washed with isopropanol and MilliQ water, and the deprotected ridges were functionalized with the 1 mM amine reactive SNAP- or CLIP-tag substrate (respectively BG-GLA-NHS or BC-GLA-NHS), to which the SNAP- or CLIP-tag protein can covalently bind. To facilitate cell adhesion to the chip, remaining PhSNPPOC groups were removed by flood exposure and the free binding sites were functionalized with the hetero-bifunctional crosslinker azido-PEG4-NHS, to which the extracellular matrix-mimicking peptide GRGDSPGSC-(DBCO) was coupled. The setup and phase mask used to generate template mologram was a kind gift of Roche (Basel, Switzerland).

Molographic Cell Measurements. Cells stably expressing Grb2- or pE59-BioMeRs were grown to 60−80% confluency in T25 culture flasks. Cells that were stimulated with the cell-penetrating peptide were starved in FBS-free media overnight. Cells were washed twice with warm PBS, incubated with 1x versene for 5 min and gently resuspended in a warm cell culture medium. The cells were then centrifuged at 50 rcf for 1 min and resuspended in media two times sequentially to minimize cellular debris. Cells were seeded on the molographic chip in an incubation chamber containing 500 μL of cell culture media. Note, the cells were only seeded when their viability exceeded 90%, as determined by a Countess automated cell counter (Invitrogen). The cells were kept in a CO_2 incubator at 37 °C for 2 h to allow cell adherence to the sensor chip (and covalent interaction of the SNAP- or CLIP-tag of the BioMeRs with the substrate on the chip). The incubation chamber containing the cells was then washed twice with warm HBSS buffer (supplemented with 20 mM HEPES, pH 7.4), adjusted for DMSO if needed and transferred to a modified F3000 ZeptoReader (Zeptosens), which was kept at 35 °C. The molographic chip was allowed to temperature-equilibrate inside the ZeptoReader for 5−10 min before performing the assay. For all molographic assays, the signal was monitored for 7−10 min (baseline measurement) before addition of the respective compound. Typical instrument parameters for molographic signal acquisition were as follows: one image was acquired every 10 s using the 635 nm laser with an integration time of 0.25−1 s depending on the intensity of the initial signal and a gray filter value of 0.001 in the illumination path of the ZeptoReader. For the evaluation of the molographic signal, automation (AutoHotkey) and evaluation (MATLAB) scripts were used.[32]

Data Analysis and Calculations. As described previously,[38] the equivalent coherent mass modulation was obtained via an algorithm that computes the power in the waveguide from the scattered background intensity of the waveguide mode as described in ref 33. The anisotropy of the scattering was assumed to be 0.05418. The damping constant was computed separately for every chip and mologram field (3−6 dB/cm), and the numerical aperture of the Zeptoreader is 0.33. Because the Zeptoreader is incapable of resolving the Airy disk, the measured signal (arb. units) was divided by the expected Airy disk area to obtain a quantity that was proportional to the average intensity in the Airy disk. The quantity proportional to the background intensity was computed from the background signal (arb. units) by dividing it by the pixel size of the ZeptoReader (12.5 x 12.5 μm). The ratio of these two quantities was then used in eq 11 of ref 33 with the necessary scaling factors to obtain the equivalent coherent mass density from the average intensity in the Airy disk. The algorithm was implemented in MATLAB as well as in Python.

The number of proteins per cell was derived as follows. The equivalent coherent mass density was multiplied with the area of the mologram footprint to receive the coherent mass. We assumed that the mologram with a diameter of 400 μm was covered by about 1000 cells. However, due to the central curved recess area, BioMeRs are only aligned in about 80% of the cells to the template mologram. The coherent mass was thus divided by 800 cells to receive the coherent mass per cell. To account for imperfect alignment of the BioMeRs, the coherent mass per cell has to be divided by the analyte efficiency (0.24)[64] to receive the total mass of the proteins per cell. Dividing with the molecular weight of the protein and multiplying with Avogadro's constant then yields the number of proteins per cell.

CLSM Imaging and Segmentation. For fluorescence imaging, cells were seeded on a 24-glass bottom well plate at 50% confluence and transfected after 24 h, as described previously. The transfection medium was replaced after 12 h with a complete medium. Cells were imaged 12, 24, 36, and 48 h after transfection using an Olympus FluoView FV3000 confocal laser scanning microscope. Prior to imaging, cells were incubated with SNAP-surface 649 dye for 30 mins and then washed three times with warm PBS. During imaging, cells were kept at 37 °C with 5% CO_2. The eYFP and SNAP-Surface 649 channels were acquired simultaneously with a 20x objective using 514 nm excitation/527 nm emission wavelengths and 651 nm excitation/667 nm emission wavelengths for the green and red channels, respectively. CLSM settings were kept the same for all samples.

Acquired images were batch converted to a TIFF format using Fiji[65] and imported into Matlab for further processing. Images were first split into three different channels (bright field, green, and red). For the green and red channels, a normalized histogram of intensities was plotted using the grayscale values of each channel. The optimal threshold to distinguish between the object and background pixels was calculated for each image using the following equation:

$$T = \frac{\mu_0 + \mu_b}{2} + \frac{\sigma 2}{\mu_0 - \mu_b} \ln\left(\frac{P_b}{P_0}\right)$$

where μ_0 and μ_b are the mean values of the normal distributions of object pixels and background pixels respectively, P_0 is the probability that a pixel belongs to the object, and P_b is the probability that it belongs to the background. The above equation assumes that the variances of the Gaussian curves of object and background pixels are equal ($\sigma_0 = \sigma_b = \sigma$). The total amount of fluorescence was then calculated by summing the intensities over all object pixels in each channel. The ratio of SNAP-surface 649 (red channel) to eYFP fluorescence (green channel) was calculated by dividing the total red and green fluorescence for each image. The value of total eYFP fluorescence and the ratio between SNAP-surface 649 and eYFP fluorescence were then plotted as a box plot for Gluc, IL-2 and IgK samples at 12, 24, 36, and 48 h.

AUTHOR INFORMATION

Corresponding Author

Andreas M Reichmuth − *Laboratory of Biosensors and Bioelectronics, Institute for Biomedical Engineering, ETH Zurich, 8092 Zurich, Switzerland;* orcid.org/0000-0002-4365-2119; Email: reichmuth@biomed.ee.ethz.ch

Authors

Ilaria Incaviglia − *Laboratory of Biosensors and Bioelectronics, Institute for Biomedical Engineering, ETH Zurich, 8092 Zurich, Switzerland*

Andreas Frutiger − *Laboratory of Biosensors and Bioelectronics, Institute for Biomedical Engineering, ETH Zurich, 8092 Zurich, Switzerland*

Yves Blickenstorfer − *Laboratory of Biosensors and Bioelectronics, Institute for Biomedical Engineering, ETH Zurich, 8092 Zurich, Switzerland*

Fridolin Treindl − *Laboratory of Biosensors and Bioelectronics, Institute for Biomedical Engineering, ETH Zurich, 8092 Zurich, Switzerland*

Giulia Ammirati − *Laboratory of Biosensors and Bioelectronics, Institute for Biomedical Engineering, ETH Zurich, 8092 Zurich, Switzerland*

https://doi.org/10.1021/acssensors.0c02480
ACS Sens. 2021, 6, 1572−1582

Ines Lüchtefeld − *Laboratory of Biosensors and Bioelectronics, Institute for Biomedical Engineering, ETH Zurich, 8092 Zurich, Switzerland*

Birgit Dreier − *Department of Biochemistry, University of Zurich, 8057 Zurich, Switzerland*

Andreas Plückthun − *Department of Biochemistry, University of Zurich, 8057 Zurich, Switzerland;* orcid.org/0000-0003-4191-5306

Janos Vörös − *Laboratory of Biosensors and Bioelectronics, Institute for Biomedical Engineering, ETH Zurich, 8092 Zurich, Switzerland;* orcid.org/0000-0001-6054-6230

Complete contact information is available at: https://pubs.acs.org/10.1021/acssensors.0c02480

Notes

The authors declare the following competing financial interest(s): A.M.R., I.I., Y.B., I.L., F.T., and J.V. declare that they have no competing financial interests. A.F. is involved with the commercialization of focal molography. A.P. is involved with the commercialization of the DARPin technology.

■ ACKNOWLEDGMENTS

We acknowledge the Roche Innovation Center in Basel, and Christof Fattinger in particular, for providing the molographic chips and the experimental setup that we used for synthesis of mologrames by reactive immersion lithography. Furthermore, we thank Prof. Paola Picotti (ETH), Prof. Matthias Peter (ETH), and Prof. Olivier Pertz (University of Bern) as well as Dr. Maria Waldhoer (Interax), Dr. Maciej Dobrzynski (University of Bern), Dr. Nako Nakatsuka (ETH), Dr. Stephanie Hwu (ETH), and Aline F Renz (ETH) for helpful discussions on the topic. Finally, we thank Linda Molli (University of Pisa) for proofreading the manuscript.

■ REFERENCES

(1) LaCount, D. J.; Vignali, M.; Chettier, R.; Phansalkar, A.; Bell, R.; Hesselberth, J. R.; Schoenfeld, L. W.; Ota, I.; Sahasrabudhe, S.; Kurschner, C.; Fields, S.; Hughes, R. E. A Protein Interaction Network of the Malaria Parasite Plasmodium Falciparum. *Nature* **2005**, *438*, 103−107.

(2) Krogan, N. J.; Cagney, G.; Yu, H.; Zhong, G.; Guo, X.; Ignatchenko, A.; Li, J.; Pu, S.; Datta, N.; Tikuisis, A. P.; Punna, T.; Peregrín-Alvarez, J. M.; Shales, M.; Zhang, X.; Davey, M.; Robinson, M. D.; Paccanaro, A.; Bray, J. E.; Sheung, A.; Beattie, B.; Richards, D. P.; Canadien, V.; Lalev, A.; Mena, F.; Wong, P.; Starostine, A.; Canete, M. M.; Vlasblom, J.; Wu, S.; Orsi, C.; Collins, S. R.; Chandran, S.; Haw, R.; Rilstone, J. J.; Gandi, K.; Thompson, N. J.; Musso, G.; St Onge, P.; Ghanny, S.; Lam, M. H. Y.; Butland, G.; Altaf-Ul, A. M.; Kanaya, S.; Shilatifard, A.; O'Shea, E.; Weissman, J. S.; Ingles, C. J.; Hughes, T. R.; Parkinson, J.; Gerstein, M.; Wodak, S. J.; Emili, A.; Greenblatt, J. F. Global Landscape of Protein Complexes in the Yeast Saccharomyces Cerevisiae. *Nature* **2006**, *440*, 637−643.

(3) Komurov, K.; White, M. Revealing Static and Dynamic Modular Architecture of the Eukaryotic Protein Interaction Network. *Mol. Syst. Biol.* **2007**, *3*, 110.

(4) Oprea, T. I.; Bologa, C. G.; Brunak, S.; Campbell, A.; Gan, G. N.; Gaulton, A.; Gomez, S. M.; Guha, R.; Hersey, A.; Holmes, J.; Jadhav, A.; Jensen, L. J.; Johnson, G. L.; Karlson, A.; Leach, A. R.; Ma'ayan, A.; Malovannaya, A.; Mani, S.; Mathias, S. L.; McManus, M. T.; Meehan, T. F.; von Mering, C.; Muthas, D.; Nguyen, D.-T.; Overington, J. P.; Papadatos, G.; Qin, J.; Reich, C.; Roth, B. L.; Schürer, S. C.; Simeonov, A.; Sklar, L. A.; Southall, N.; Tomita, S.; Tudose, I.; Ursu, O.; Vidovic, D.; Waller, A.; Westergaard, D.; Yang, J. J.; Zahoránszky-Köhalmi, G. Unexplored Therapeutic Opportunities in the Human Genome. *Nat. Rev. Drug Discov.* **2018**, *17*, 317−332.

(5) Conte, L. L.; Chothia, C.; Janin, J. The Atomic Structure of Protein-Protein Recognition sites. *J. Mol. Biol.* **1999**, *285*, 2177−2198.

(6) Scott, D. E.; Ehebauer, M. T.; Pukala, T.; Marsh, M.; Blundell, T. L.; Venkitaraman, A. R.; Abell, C.; Hyvönen, M. Using a Fragment-Based Approach to Target Protein-Protein Interactions. *ChemBioChem* **2013**, *14*, 332−342.

(7) Krüger, D. M.; Jessen, G.; Gohlke, H. How Good Are State-of-the-Art Docking Tools in Predicting Ligand Binding Modes in Protein-Protein Interfaces? *J. Chem. Inf. Model.* **2012**, *52*, 2807−2811.

(8) Lo, M.-C.; Aulabaugh, A.; Jin, G.; Cowling, R.; Bard, J.; Malamas, M.; Ellestad, G. Evaluation of Fluorescence-Based Thermal Shift Assays for Hit Identification in Drug Discovery. *Anal. Biochem.* **2004**, *332*, 153−159.

(9) Davies, T. G.; Tickle, I. J. Fragment Screening Using X-Ray Crystallography. *Top. Curr. Chem.* **2012**, *317*, 33−59.

(10) Navratilova, I.; Hopkins, A. L. Emerging Role of Surface Plasmon Resonance in Fragment-Based Drug Discovery. *Future Med. Chem.* **2011**, *3*, 1809−1820.

(11) Harner, M. J.; Frank, A. O.; Fesik, S. W. Fragment-Based Drug Discovery Using NMR Spectroscopy. *J. Biomol. NMR* **2013**, *56*, 65−75.

(12) Wedeking, T.; Löchte, S.; Richter, C. P.; Bhagawati, M.; Piehler, J.; You, C. Single Cell GFP-Trap Reveals Stoichiometry and Dynamics of Cytosolic Protein Complexes. *Nano Lett.* **2015**, *15*, 3610−3615.

(13) Jain, A.; Liu, R.; Ramani, B.; Arauz, E.; Ishitsuka, Y.; Ragunathan, K.; Park, J.; Chen, J.; Xiang, Y. K.; Ha, T. Probing Cellular Protein Complexes Using Single-Molecule Pull-Down. *Nature* **2011**, *473*, 484−488.

(14) Ryu, J. Y.; Kim, J.; Shon, M. J.; Sun, J.; Jiang, X.; Lee, W.; Yoon, T.-Y. Profiling Protein-Protein Interactions of Single Cancer Cells with in Situ Lysis and Co-Immunoprecipitation. *Lab Chip* **2019**, *19*, 1922−1928.

(15) Sekar, R. B.; Periasamy, A. Fluorescence Resonance Energy Transfer (FRET) Microscopy Imaging of Live Cell Protein Localizations. *J. Cell Biol.* **2003**, *160*, 629−633.

(16) Bacart, J.; Corbel, C.; Jockers, R.; Bach, S.; Couturier, C. The BRET Technology and Its Application to Screening Assays. *Biotechnol. J.* **2008**, *3*, 311−324.

(17) Lavoie, H.; Thevakumaran, N.; Gavory, G.; Li, J. J.; Padeganeh, A.; Guiral, S.; Duchaine, J.; Mao, D. Y. L.; Bouvier, M.; Sicheri, F.; Therrien, M. Inhibitors That Stabilize a Closed RAF Kinase Domain Conformation Induce Dimerization. *Nat. Chem. Biol.* **2013**, *9*, 428−436.

(18) Wu, P. G.; Brand, L. Resonance Energy Transfer: Methods and Applications. *Anal. Biochem.* **1994**, *218*, 1−13.

(19) Newman, R. H.; Fosbrink, M. D.; Zhang, J. Genetically Encodable Fluorescent Biosensors for Tracking Signaling Dynamics in Living Cells. *Chem. Rev.* **2011**, *111*, 3614−3666.

(20) Midtvedt, D.; Olsén, E.; Höök, F.; Jeffries, G. D. M. Label-Free Spatio-Temporal Monitoring of Cytosolic Mass, Osmolarity, and Volume in Living Cells. *Nat. Commun.* **2019**, *10*, 340.

(21) Fang, Y.; Ferrie, A. M.; Fontaine, N. H.; Mauro, J.; Balakrishnan, J. Resonant Waveguide Grating Biosensor for Living Cell Sensing. *Biophys. J.* **2006**, *91*, 1925−1940.

(22) Ciambrone, G. J.; Liu, V. F.; Lin, D. C.; McGuinness, R. P.; Leung, G. K.; Pitchford, S. Cellular Dielectric Spectroscopy: A Powerful New Approach to Label-Free Cellular Analysis. *J. Biomol. Screening* **2004**, *9*, 467−480.

(23) Schröder, R.; Janssen, N.; Schmidt, J.; Kebig, A.; Merten, N.; Hennen, S.; Müller, A.; Blättermann, S.; Mohr-Andrä, M.; Zahn, S.; Wenzel, J.; Smith, N. J.; Gomeza, J.; Drewke, C.; Milligan, G.; Mohr, K.; Kostenis, E. Deconvolution of Complex G Protein-Coupled Receptor Signaling in Live Cells Using Dynamic Mass Redistribution Measurements. *Nat. Biotechnol.* **2010**, *28*, 943−949.

(24) Grundmann, M.; Merten, N.; Malfacini, D.; Inoue, A.; Preis, P.; Simon, K.; Rüttiger, N.; Ziegler, N.; Benkel, T.; Schmitt, N. K.; Ishida,

S.; Müller, I.; Reher, R.; Kawakami, K.; Inoue, A.; Rick, U.; Kühl, T.; Imhof, D.; Aoki, J.; König, G. M.; Hoffmann, C.; Gomeza, J.; Wess, J.; Kostenis, E. Lack of Beta-Arrestin Signaling in the Absence of Active G Proteins. *Nat. Commun.* **2018**, *9*, 341.
(25) Kurucz, I.; Peter, B.; Prosz, A.; Szekacs, I.; Horvath, R.; Erdei, A. Label-Free Optical Biosensor for on-Line Monitoring the Integrated Response of Human B Cells upon the Engagement of Stimulatory and Inhibitory Immune Receptors. *Sens. Actuators, B* **2017**, *240*, 528−535.
(26) Klein, A. B.; Nittegaard-Nielsen, M.; Christensen, J. T.; Al-Khawaja, A.; Wellendorph, P. Demonstration of the Dynamic Mass Redistribution Label-Free Technology as a Useful Cell-Based Pharmacological Assay for Endogenously Expressed $GABA_A$ Receptors. *Med. Chem. Commun.* **2016**, *7*, 426−432.
(27) Krebs, K. M.; Pfeil, E. M.; Simon, K.; Grundmann, M.; Häberlein, F.; Bautista-Aguilera, O. M.; Gütschow, M.; Weaver, C. D.; Fleischmann, B. K.; Kostenis, E. Label-Free Whole Cell Biosensing for High-Throughput Discovery of Activators and Inhibitors Targeting G Protein-Activated Inwardly Rectifying Potassium Channels. *ACS Omega* **2018**, *3*, 14814−14823.
(28) Orgovan, N.; Ungai-Salánki, R.; Lukácsi, S.; Sándor, N.; Bajtay, Z.; Erdei, A.; Szabó, B.; Horvath, R. Adhesion Kinetics of Human Primary Monocytes, Dendritic Cells, and Macrophages: Dynamic Cell Adhesion Measurements with a Label-Free Optical Biosensor and Their Comparison with End-Point Assays. *Biointerphases* **2016**, *11*, No. 031001.
(29) Szekacs, I.; Farkas, E.; Gemes, B. L.; Takacs, E.; Szekacs, A.; Horvath, R. Integrin Targeting of Glyphosate and Its Cell Adhesion Modulation Effects on Osteoblastic MC3T3-E1 Cells Revealed by Label-Free Optical Biosensing. *Sci. Rep.* **2018**, *8*, 17401.
(30) Szekacs, I.; Orgovan, N.; Peter, B.; Kovacs, B.; Horvath, R. Receptor Specific Adhesion Assay for the Quantification of Integrin−ligand Interactions in Intact Cells Using a Microplate Based, Label-Free Optical Biosensor. *Sens. Actuators, B* **2018**, *256*, 729−734.
(31) Fattinger, C. Focal Mology: Coherent Microscopic Detection of Biomolecular Interaction. *Phys. Rev. X* **2014**, *4*, No. 031024.
(32) Gatterdam, V.; Frutiger, A.; Stengele, K.-P.; Heindl, D.; Lübbers, T.; Vörös, J.; Fattinger, C. Focal Mology Is a New Method for the in Situ Analysis of Molecular Interactions in Biological Samples. *Nat. Nanotechnol.* **2017**, 1089.
(33) Frutiger, A.; Blickenstorfer, Y.; Bischof, S.; Forró, C.; Lauer, M.; Gatterdam, V.; Fattinger, C.; Vörös, J. Principles for Sensitive and Robust Biomolecular Interaction Analysis: The Limits of Detection and Resolution of Diffraction-Limited Focal Mology. *Phys. Rev. Appl.* **2019**, *11*, No. 014056.
(34) Reichmuth, A. M.; Kübrich, K.; Blickenstorfer, Y.; Frutiger, A.; Momotenko, D.; Gatterdam, V.; Treindl, F.; Fattinger, C.; Vörös, J. Investigating Complex Samples with Mologrames of Low-Affinity Binders. *ACS Sens* **2021**, DOI: 10.1021/acssensors.0c02346.
(35) Frutiger, A.; Gatterdam, K.; Blickenstorfer, Y.; Reichmuth, A. M.; Fattinger, C.; Vörös, J. Ultra Stable Molecular Sensors by Submicron Referencing and Why They Should Be Interrogated by Optical Diffraction-Part II. Experimental Demonstration. *Sensors* **2021**, *21*, 9.
(36) Frutiger, A.; Fattinger, C.; Vörös, J. Ultra-Stable Molecular Sensors by Sub-Micron Referencing and Why They Should Be Interrogated by Optical Diffraction—Part I. The Concept of a Spatial Affinity Lock-in Amplifier. *Sensors* **2021**, *21*, 469.
(37) Blickenstorfer, Y.; Müller, M.; Dreyfus, R.; Reichmuth, A. M.; Fattinger, C.; Frutiger, A. Quantitative Diffractometric Biosensing. *Phys. Rev. Appl.* **2020**, 034023 15052. arXiv. https://arxiv.org/abs/2011.15052 (accessed 02 17, 2021).
(38) Reichmuth, A. M.; Zimmermann, M.; Wilhelm, F.; Frutiger, A.; Blickenstorfer, Y.; Fattinger, C.; Waldhoer, M.; Vörös, J. Quantification of Molecular Interactions in Living Cells in Real Time Using a Membrane Protein Nanopattern. *Anal. Chem.* **2020**, 8983.
(39) Schröder, R.; Schmidt, J.; Blättermann, S.; Peters, L.; Janssen, N.; Grundmann, M.; Seemann, W.; Kaufel, D.; Merten, N.; Drewke, C.; Gomeza, J.; Milligan, G.; Mohr, K.; Kostenis, E. Applying Label-Free Dynamic Mass Redistribution Technology to Frame Signaling of G Protein-Coupled Receptors Noninvasively in Living Cells. *Nat. Protoc.* **2011**, *6*, 1748−1760.
(40) Du, Y.; Li, Z.; Li, L.; Chen, Z. G.; Sun, S.-Y.; Chen, P.; Shin, D. M.; Khuri, F. R.; Fu, H. Distinct Growth Factor-Induced Dynamic Mass Redistribution (DMR) Profiles for Monitoring Oncogenic Signaling Pathways in Various Cancer Cells. *J. Recept. Signal Transduct. Res.* **2009**, *29*, 182−194.
(41) Gandor, S.; Reisewitz, S.; Venkatachalapathy, M.; Arrabito, G.; Reibner, M.; Schröder, H.; Ruf, K.; Niemeyer, C. M.; Bastiaens, P. I. H.; Dehmelt, L. A Protein-Interaction Array inside a Living Cell. *Angew. Chem., Int. Ed Engl.* **2013**, *52*, 4790−4794.
(42) Waldo, G. S.; Standish, B. M.; Berendzen, J.; Terwilliger, T. C. Rapid Protein-Folding Assay Using Green Fluorescent Protein. *Nat. Biotechnol.* **1999**, *17*, 691−695.
(43) Cymer, F.; von Heijne, G.; White, S. H. Mechanisms of Integral Membrane Protein Insertion and Folding. *J. Mol. Biol.* **2015**, *427*, 999−1022.
(44) Zhang, L.; Leng, Q.; Mixson, A. J. Alteration in the IL-2 Signal Peptide Affects Secretion of Proteins in Vitro and in Vivo. *J. Gene Med.* **2005**, *7*, 354−365.
(45) Knappskog, S.; Ravneberg, H.; Gjerdrum, C.; Trö*β*e, C.; Stern, B.; Pryme, I. F. The Level of Synthesis and Secretion of Gaussia Princeps Luciferase in Transfected CHO Cells Is Heavily Dependent on the Choice of Signal Peptide. *J. Biotechnol.* **2007**, *128*, 705−715.
(46) Kober, L.; Zehe, C.; Bode, J. Optimized Signal Peptides for the Development of High Expressing CHO Cell Lines. *Biotechnol. Bioeng.* **2013**, *110*, 1164−1173.
(47) Plückthun, A. Designed Ankyrin Repeat Proteins (DARPins): Binding Proteins for Research, Diagnostics, and Therapy. *Annu. Rev. Pharmacol. Toxicol.* **2015**, *55*, 489−511.
(48) Petsalaki, E.; Russell, R. B. Peptide-Mediated Interactions in Biological Systems: New Discoveries and Applications. *Curr. Opin. Biotechnol.* **2008**, *19*, 344−350.
(49) London, N.; Raveh, B.; Schueler-Furman, O. Druggable Protein-Protein Interactions–from Hot Spots to Hot Segments. *Curr. Opin. Chem. Biol.* **2013**, *17*, 952−959.
(50) Arkin, M. R.; Tang, Y.; Wells, J. A. Small-Molecule Inhibitors of Protein-Protein Interactions: Progressing toward the Reality. *Chem. Biol.* **2014**, *21*, 1102−1114.
(51) Matsson, P.; Doak, B. C.; Over, B.; Kihlberg, J. Cell Permeability beyond the Rule of 5. *Adv. Drug Delivery Rev.* **2016**, *101*, 42−61.
(52) Tari, A. M.; Lopez-Berestein, G. GRB2: A Pivotal Protein in Signal Transduction. *Semin. Oncol.* **2001**, *28*, 142−147.
(53) Lowenstein, E. J.; Daly, R. J.; Batzer, A. G.; Li, W.; Margolis, B.; Lammers, R.; Ullrich, A.; Skolnik, E. Y.; Bar-Sagi, D.; Schlessinger, J. The SH2 and SH3 Domain-Containing Protein GRB2 Links Receptor Tyrosine Kinases to Ras Signaling. *Cell* **1992**, *70*, 431−442.
(54) Giubellino, A.; Burke, T. R., Jr.; Bottaro, D. P. Grb2 Signaling in Cell Motility and Cancer. *Expert Opin. Ther. Targets* **2008**, *12*, 1021−1033.
(55) Kardinal, C.; Konkol, B.; Lin, H.; Eulitz, M.; Schmidt, E. K.; Estrov, Z.; Talpaz, M.; Arlinghaus, R. B.; Feller, S. M. Chronic Myelogenous Leukemia Blast Cell Proliferation Is Inhibited by Peptides That Disrupt Grb2-SoS Complexes. *Blood* **2001**, *98*, 1773−1781.
(56) Lemmon, M. A.; Schlessinger, J. Cell Signaling by Receptor Tyrosine Kinases. *Cell* **2010**, *141*, 1117−1134.
(57) Cohen, P. The Regulation of Protein Function by Multisite Phosphorylation–a 25 Year Update. *Trends Biochem. Sci.* **2000**, *25*, 596−601.
(58) Hunter, T. Protein Kinases and Phosphatases: The Yin and Yang of Protein Phosphorylation and Signaling. *Cell* **1995**, *80*, 225−236.
(59) Lyon, K.; Stasevich, T. J. Imaging Translational and Post-Translational Gene Regulatory Dynamics in Living Cells with Antibody-Based Probes. *Trends Genet.* **2017**, *33*, 322−335.

(60) Cattaneo, A.; Chirichella, M. Targeting the Post-Translational Proteome with Intrabodies. *Trends Biotechnol.* **2019**, *37*, 578−591.
(61) Kummer, L.; Parizek, P.; Rube, P.; Millgramm, B.; Prinz, A.; Mittl, P. R. E.; Kaufholz, M.; Zimmermann, B.; Herberg, F. W.; Plückthun, A. Structural and Functional Analysis of Phosphorylation-Specific Binders of the Kinase ERK from Designed Ankyrin Repeat Protein Libraries. *Proc. Natl. Acad. Sci. U. S. A.* **2012**, *109*, E2248−E2257.
(62) Kummer, L.; Hsu, C.-W.; Dagliyan, O.; MacNevin, C.; Kaufholz, M.; Zimmermann, B.; Dokholyan, N. V.; Hahn, K. M.; Plückthun, A. Knowledge-Based Design of a Biosensor to Quantify Localized ERK Activation in Living Cells. *Chem. Biol.* **2013**, *20*, 847−856.
(63) Ryu, H.; Chung, M.; Dobrzyński, M.; Fey, D.; Blum, Y.; Lee, S. S.; Peter, M.; Kholodenko, B. N.; Jeon, N. L.; Pertz, O. Frequency Modulation of ERK Activation Dynamics Rewires Cell Fate. *Mol. Syst. Biol.* **2015**, *11*, 838.
(64) Frutiger, A.; Tschannen, C. D.; Blickenstorfer, Y.; Reichmuth, A. M.; Fattinger, C.; Vörös, J. Image Reversal Reactive Immersion Lithography Improves the Detection Limit of Focal Molography. *Opt. Lett.* **2018**, *43*, 5801−5804.
(65) Schindelin, J.; Arganda-Carreras, I.; Frise, E.; Kaynig, V.; Longair, M.; Pietzsch, T.; Preibisch, S.; Rueden, C.; Saalfeld, S.; Schmid, B.; Tinevez, J.-Y.; White, D. J.; Hartenstein, V.; Eliceiri, K.; Tomancak, P.; Cardona, A. Fiji: An Open-Source Platform for Biological-Image Analysis. *Nat. Methods* **2012**, *9*, 676−682.

https://doi.org/10.1021/acssensors.0c02480
ACS Sens. 2021, 6, 1572−1582